Speed Measurement Error Suppression for PMSM Control System Using Self-Adaption Kalman Observer

Tingna Shi, *Member, IEEE*, Zheng Wang, and Changliang Xia, *Senior Member, IEEE*

***Abstract*—This paper proposes a self-adaption Kalman observer (SAKO) used in a permanent-magnet synchronous motor (PMSM) servo system. The proposed SAKO can make up measurement noise of the absolute encoder with limited resolution ratio and avoid differentiating process and filter delay of the traditional speed measuring methods. To be different from the traditional Kalman observer, the proposed observer updates the gain matrix by calculating the measurement noise at the current time. The variable gain matrix is used to estimate and correct the observed position, speed, and load torque to solve the problem that the motor speed calculated by the traditional methods is prone to large speed error and time delay when PMSM runs at low speeds. The state variables observed by the proposed observer are used as the speed feedback signals and compensation signal of the load torque disturbance in PMSM servo system. The simulations and experiments prove that the SAKO can observe speed and load torque precisely and timely and that the feedforward and feedback control system of PMSM can improve the speed tracking ability.**

***Index Terms*—Feedforward control, Kalman observer (KO), measurement noise, permanent-magnet synchronous motor (PMSM), speed estimation.**

I. Introduction

THE permanent-magnet synchronous motor (PMSM) has been widely used in the field of high-performance control due to its high power factor, good speed control performance, etc. For PMSM servo system, rotor position and speed are necessary feedback signals in the closed control system. In traditional methods of position measurement, the position signal is usually obtained by an optical encoder that includes an incremental encoder, an absolute encoder, and a hybrid encoder. In the vector control of PMSM system, coordinate transformation is necessary to transform the variables in abc three-phase coordinate system to those in dq rotating coordinate system. In this process, the absolute position of the rotor is indispensable, particularly when the motor starts up. Therefore, it is a good choice to equip the motor with an absolute encoder, which can ensure the motor starts up normally in a convenient and fast way. In addition, absolute encoder not only has obvious advantages in anti-interference ability, location ability, etc., but it can also obtain the binary coding of the absolute rotor position, which renders it being widely used in many high precise places (e.g., mechanical equipments).

Recently, the analyses and studies about speed measuring methods and speed precision mainly focus on incremental encoder [1]–[3], and the studies on absolute encoder mainly focus on the design and analysis aspects [4]–[6]. Due to quantization noise, the nonideal manufacture of optical encoders, and other reasons, the rotor position measured by optical encoder has measurement noise, causing some errors in the speed calculated by rotor position signal. In addition, traditional speed measuring methods such as M method, T method, and M/T method all calculate average speed based on derivation algorithm, giving rise to time delay and speed error that is called speed noise. The speed noise influences both the dynamic and steady performances and stability of PMSM servo system to some extent [7]. Although low filters are usually used to restrain speed noise, they cannot decrease time delay at the same time [8], [9].

A high-precision encoder can improve the precision of speed measuring methods, although the cost of it is relatively high. To avoid the shortcomings of traditional speed measuring methods, scholars propose many ways to estimate speed, such as nonlinear observers [10], [11] and sliding mode observers [12]–[14]. Among them, the authors in [15] deem that numerical integration can provide more stable and accurate results than numerical differentiation in the presence of noise. In addition, an enhanced differentiator is proposed to improve velocity estimation in low-speed regions. The authors in [16] propose a neural-based full-order Luenberger adaptive speed observer for sensorless linear induction motor drives whose linear speed is estimated with the TLS EXIN neuron. The authors in [17] introduce an adaptive interconnected observer for sensorless control of a synchronous motor, which is used to estimate the rotor speed, rotor position, and load torque. Since the speed is not calculated in every sampling period when the motor runs at a low speed, in order to ensure the update of the speed in each sampling period, an instantaneous speed observer is used in [18], which estimate the speed in each sampling period and correct the estimation

Manuscript received April 14, 2014; revised July 1, 2014 and September 15, 2014; accepted October 2, 2014. Date of publication October 24, 2014; date of current version April 8, 2015. This work was supported in part by a project funded by the National Key Basic Research Program of China (973 project) under Grant 2013CB035600 and in part by the Key Technologies Research and Development Program of Tianjin under Grant 13ZCZDGX01100.

T. Shi and Z. Wang are with the School of Electrical Engineering and Automation, Tianjin University, Tianjin 300072, China (e-mail: tnshi@tju.edu.cn; wzheng0614@tju.edu.cn).

C. Xia is with the School of Electrical Engineering and Automation, Tianjin University, Tianjin 300072, China, and also with the Tianjin Key Laboratory of Advanced Technology of Electrical Engineering and Energy, Tianjin Polytechnic University, Tianjin 300387, China (e-mail: motor@tju.edu.cn).

Color versions of one or more of the figures in this paper are available online at http://ieeexplore.ieee.org.

Digital Object Identifier 10.1109/TIE.2014.2364989

error when the position is updated. In [19] and [20], a full-order observer or a reduced-order observer that needs a precise mathematical model of the motor is proposed to observe the speed. A robust digital differentiator that provides the first derivative of the encoder position measurement is proposed to observe speed in [21]. Since Kalman filtering algorithm is an optimum estimation method in the sense of variance minimizing, it can use recursive method to process the random noise interference directly and have lower dependence on the model [22]. As a result, Kalman observer (KO) is widely used to observe the system speed [23]–[25].

Since the position error of the optical encoder can be regarded as Gaussian white noise [26], [27], the optimal estimation of the speed and load torque can be obtained by Kalman filter from a series of position signals with noises. In order to make the estimations correct, a SAKO is proposed to accurately observe position, speed, and load torque. By analyzing quantization error of absolute encoder, measurement noise of the system is calculated based on the variation of the rotor position and reflects the actual process. Then instantaneous speed observer and KO are combined together to decrease the influence of the measurement error on the observed speed when the sampling time does not match the update time of the position. Finally, the observed signals are used as speed feedback signals and compensation signal of load torque disturbance, thereby constructing a feedforward and feedback control system of PMSM.

II. Speed Error Analysis of Absolute Encoder

The code disk of n-bit absolute encoder is covered with n circles of uniformly distributed grooves, which are either light transmitting or non-light transmitting. The values of adjacent code channels are arrayed according to certain rules that every radial position has only one binary coding associated with them, the range of which is $0 \sim 2^n - 1$. The resolution ratio of n-bit absolute encoder is $1/2^n$. This is to say that the $2\pi\text{rad}$ circumference is dispersed to a series of position signals, the gap among which is $2\pi/2^n\text{rad}$.

Fig. 1(a) and (b) shows the signal curves at low and high speeds, respectively. The signals include the continuous actual rotor position, the position signal identified by the absolute encoder, and the position signal that is exported by the absolute encoder and read by a digital signal processor (DSP). For the convenience of analyzing, the speed is assumed to be a constant value that is larger than zero.

In Fig. 1, k is the sampling number, $k = 1, 2, \ldots$; θ is the rotor position; $\theta(m)$ is the rotor position that DSP reads out in the mth time, $m = 1, 2, \ldots$; $\Delta\theta(m)$ is the measurement error, i.e., the difference between the actual rotor position and $\theta(m)$; $\dot{\theta}$ is the derivative of the rotor position, namely, speedω; T_s is the sampling time of the controllers; T_{1_actual} is the time interval between two consecutive position updates identified by the absolute encoder; and T_1 is the time interval between two consecutive position updates read by DSP.

As shown in Fig. 1, the absolute encoder obtains discrete position when the variation of rotor position is equal to quantization error $\Delta = 2\pi/2^n\text{rad}$; however, the new position is read by

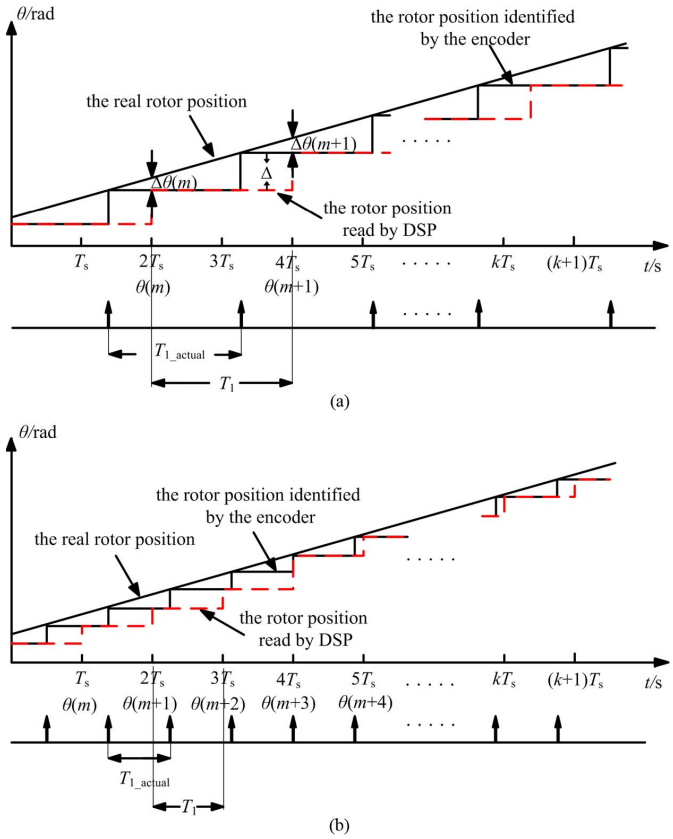

Fig. 1. Curves of rotor position signal (a) when the motor runs at a low speed, i.e., $T_{1\_\text{actual}} > T_\text{s}$, $T_1 > T_\text{s}$, and (b) when the motor runs at a high speed, i.e., $T_{1\_\text{actual}} < T_\text{s}$, $T_1 = T_\text{s}$.

DSP only when the next sampling signal comes, which causes the measurement error between the actual position and that read by DSP. The maximum measurement error happens when the sampling occurs just before the encoder identifies a new position, and it equals to quantization error $\Delta = 2\pi/2^n\text{rad}$; whereas the minimum occurs when the sampling coincides with the moment that the encoder identifies a new position, and its value is zero.

As shown in Fig. 1(a), when the motor runs at a low speed, the rotor position changes slowly, and the time interval between two consecutive position updates identified by the absolute encoder T_{1_actual} becomes larger than sampling time T_s, which is a constant value. In this case, the time interval between two consecutive position updates read by DSP T_1 is larger than T_s. As shown in Fig. 1(b), when the motor runs at a high speed and the rotor position changes fast, $T_{1\_\text{actual}} < T_\text{s}$ and $T_1 = T_\text{s}$.

The speed signal is calculated by differentiating the rotor position read by the DSP. In addition, traditional speed measuring methods such as Euler method (EM), period-varying method (PVM), and period-overlapping method (POM) all calculate speed by using forward difference approximation method instead of derivation algorithm directly.

A. EM

EM based on Euler algorithm calculates the average speed using position variation and time instant that is a measurement

period equal to T_1, and the calculation equation is shown as follows:

$$\omega(m) = \frac{\theta(m) - \theta(m-1)}{T_m} \tag{1}$$

where T_m is the time interval between the $(m-1)$th and the mth variations of rotor position, and $T_m = T_1$.

Judging from Fig. 1(a), the speed error of EM $err_{\mathrm{EM}}(m)$ is as follows:

$$err_{\mathrm{EM}}(m) = \frac{\Delta\theta(m) - \Delta\theta(m-1)}{T_m}. \tag{2}$$

As the measurement error is a stochastic variable that has no relationship with T_s, it can be regarded as a uniform probability distribution in the scope of $0 \sim \Delta$; its distribution density is inversely proportional to the scope. In order to compare the errors of different speed measuring methods, the time interval between two consecutive position updates read by DSP T_1 is regarded as a constant value. The scope, expected error, and distribution density of $err_{\mathrm{EM}}(m)$ are respectively shown as follows:

$$\begin{cases} err_{\mathrm{EM}}(m) \in \left[-\frac{\Delta}{T_1}, \frac{\Delta}{T_1}\right] \\ E[err_{\mathrm{EM}}] = 0 \\ f(err_{\mathrm{EM}}) = \frac{T_1}{2\Delta}. \end{cases} \tag{3}$$

Error variance R_{EM} is

$$R_{\mathrm{EM}} = E\left[(err_{\mathrm{EM}} - E[err_{\mathrm{EM}}]) \cdot (err_{\mathrm{EM}} - E[err_{\mathrm{EM}}])^T\right] = \frac{\Delta^2}{3T_1^2}. \tag{4}$$

According to (3) and (4), EM uses position variation and time interval in a measurement period to calculate speed. Consequently, the speed calculated by EM has a large speed error.

B. PVM

In order to decrease the speed error in EM, the deviation between the first and the last positions and the time intervals in several measurement periods are used to calculate speed. In other words, the speed error is decreased by increasing the measurement periods. This method is named as PVM, and the calculation equation is shown as follows:

$$\omega(m) = \frac{\sum_{h=j+1}^{m} \theta(h) - \theta(h-1)}{\sum_{h=j+1}^{m} T_h} = \frac{\theta(m) - \theta(j)}{\sum_{h=j+1}^{m} T_h} \tag{5}$$

where j is the jth variation of the position read by DSP, whose value is a positive integer smaller than m; the value of $m-j$ is chosen by the speed, i.e., it is chosen smaller at a low speed and larger at a high speed; and T_h is the time interval between the $(m-1)$th and the hth variations of rotor position.

Likewise, the scope $err_{\mathrm{PVM}}(m)$ and error variance R_{PVM} of PVM are

$$\begin{cases} err_{\mathrm{PVM}}(m) \in \left[-\frac{\Delta}{(m-j)T_1}, \frac{\Delta}{(m-j)T_1}\right] \\ R_{\mathrm{PVM}} = \frac{\Delta^2}{3[(m-j)T_1]^2}. \end{cases} \tag{6}$$

Judging from (6), PVM improves the speed precision by increasing the measurement periods, but it causes more time delay.

C. POM

In order to shorten time delay in PVM, the speeds calculated by PVM in the current and several backward measurement periods are averaged as the speed in the current period. This method is called POM. The calculation equation is shown as follows:

$$\omega(m) = \frac{1}{v}\sum_{z=0}^{v-1}\left(\frac{\theta(m-z) - \theta(j-z)}{\sum_{h=j-z+1}^{m-z} T_h}\right) \tag{7}$$

where j is a positive integer smaller than m, and v is a positive integer smaller than $m-j+1$.

Likewise, the scope $err_{\mathrm{POM}}(m)$ and error variance R_{POM} of POM are

$$\begin{cases} err_{\mathrm{POM}}(m) \in \left[-\frac{\Delta}{(m-j)T_1}, \frac{\Delta}{(m-j)T_1}\right] \\ R_{\mathrm{POM}} = \frac{\Delta^2}{3v[(m-j)T_1]^2}. \end{cases} \tag{8}$$

A compromise between speed precision and time delay is achieved by choosing the parameters reasonably in POM.

The above three methods calculate speed only when DSP consecutively reads new position signals, rather than in each sampling period. Thus, the speeds calculated by above methods inevitably have some errors and time delays.

III. Design of SAKO

A. Design of a SAKO Based on the Model of PMSM

The motion equations of PMSM are shown as follows:

$$\begin{bmatrix} \dot{\theta} \\ \dot{\omega} \\ \dot{T}_{\mathrm{L}} \end{bmatrix} = \begin{bmatrix} 0 & 1 & 0 \\ 0 & -\frac{f}{J} & -\frac{1}{J} \\ 0 & 0 & 0 \end{bmatrix} \begin{bmatrix} \theta \\ \omega \\ T_{\mathrm{L}} \end{bmatrix} + \begin{bmatrix} 0 \\ \frac{K_{\mathrm{T}}}{J} \\ 0 \end{bmatrix} i_{\mathrm{q}} \tag{9}$$

where ω is the mechanical angular velocity; i_{q} is the current of the q-axis; J is the rotational inertia; f is the friction torque coefficient; K_{T} is the torque coefficient; and T_{L} is the load torque that is regarded as a constant in a measurement period, namely, $\dot{T}_{\mathrm{L}} = 0$.

After discretizing (9), KO can be designed as follows:

$$\begin{cases} \boldsymbol{x}(k+1) = \boldsymbol{A}\boldsymbol{x}(k) + \boldsymbol{B}\boldsymbol{u}(k) + \boldsymbol{w}(k) \\ \boldsymbol{y}(k) = \boldsymbol{C}\boldsymbol{x}(k) + \boldsymbol{r}(k) \end{cases} \tag{10}$$

where k is the sampling number; $\boldsymbol{x} = [\theta \quad \omega \quad T_{\mathrm{L}}]^{\mathrm{T}}$ is the state variant; $\boldsymbol{u} = [i_{\mathrm{q}}]$ is the control signal; $\boldsymbol{y} = [\theta]$ is the observed signal; $\boldsymbol{w}$ is the system noise, representing the influence brought by the system parameter errors; $\boldsymbol{r}$ is the measurement noise, representing measurement error and other noises in a measurement process; and coefficient matrices are

$$\boldsymbol{A} = \begin{bmatrix} 1 & T_{\mathrm{s}} & 0 \\ 0 & 1 - \frac{f}{J}T_{\mathrm{s}} & -\frac{T_{\mathrm{s}}}{J} \\ 0 & 0 & 1 \end{bmatrix}; \quad \boldsymbol{B} = \begin{bmatrix} 0 \\ \frac{T_{\mathrm{s}}K_{\mathrm{T}}}{J} \\ 0 \end{bmatrix}; \quad \boldsymbol{C} = [1\,0\,0].$$

$\boldsymbol{w}(k)$ and $\boldsymbol{r}(k)$ are identically distributed Gaussian noises, which are zero means and independent. Their covariances satisfy

$$\begin{cases} \boldsymbol{Q} = \mathrm{cov}(\boldsymbol{w}) = E[\boldsymbol{w}\boldsymbol{w}^T] \\ \boldsymbol{R} = \mathrm{cov}(\boldsymbol{r}) = E[\boldsymbol{r}\boldsymbol{r}^T] \end{cases} \tag{11}$$

where $\boldsymbol{Q}$ and $\boldsymbol{R}$ are diagonal matrices, and $\boldsymbol{r}$ and $\boldsymbol{R} = [R(k)]$ are both the first-order matrices since θ is the only observed signal.

The recursion calculation of Kalman is shown as follows:

$$\begin{cases} \boldsymbol{x}(k|k) = \boldsymbol{x}(k|k-1) + \boldsymbol{K}(k)\boldsymbol{err}(k) \\ \boldsymbol{P}(k|k) = (\boldsymbol{I} - \boldsymbol{K}(k)\boldsymbol{C})\,\boldsymbol{P}(k|k-1) \end{cases} \tag{12}$$

where all variables are at time kT_s; $\boldsymbol{x}(k|k)$ and $\boldsymbol{P}(k|k)$ are state estimate and error covariance after measurement update, respectively; $\boldsymbol{x}(k|k-1)$ and $\boldsymbol{P}(k|k-1)$ are state estimate and error covariance prior to measurement update, respectively; $\boldsymbol{I}$ is the unit matrix; and $\boldsymbol{K}(k)$ and $\boldsymbol{err}(k)$ are gain matrix and error of the observed signal, respectively. These values are updated as follows:

$$\begin{cases} \boldsymbol{x}(k|k-1) = \boldsymbol{A}\boldsymbol{x}(k-1|k-1) + \boldsymbol{B}\boldsymbol{u}(k) \\ \boldsymbol{P}(k|k-1) = \boldsymbol{A}\boldsymbol{P}(k-1|k-1)\boldsymbol{A}^\mathrm{T} + \boldsymbol{Q}(k) \\ \boldsymbol{K}(k) = \boldsymbol{P}(k|k-1)\boldsymbol{C}^\mathrm{T}\left(\boldsymbol{C}\boldsymbol{P}(k|k-1)\boldsymbol{C}^T + \boldsymbol{R}(k)\right)^{-1} \\ \boldsymbol{y}(k|k-1) = \boldsymbol{C}\boldsymbol{x}(k|k-1) \\ \boldsymbol{err}(k) = \boldsymbol{y}(k) - \boldsymbol{y}(k|k-1) \end{cases} \tag{13}$$

where $\boldsymbol{y}(k|k-1)$ is the estimate value of the observed signal at time kT_s.

Both limited precision in mathematics and the model error may lead to KO divergent in practice; therefore, in order to improve the precision of the estimation states, a suitable system noise $\boldsymbol{Q}(k)$ and a measurement noise $\boldsymbol{R}(k)$ are needed.

Judging from the above recursion equations, $\boldsymbol{Q}(k)$ and $\boldsymbol{R}(k)$ both influence $\boldsymbol{K}(k)$ and consequently affect the correction of $\boldsymbol{err}(k)$ and $\boldsymbol{x}(k|k-1)$ to $\boldsymbol{x}(k|k)$. In the traditional KO, $\boldsymbol{Q}(k)$ and $\boldsymbol{R}(k)$ are determined by trials that require many groups of repeated attempts. $\boldsymbol{K}(k)$ is convergent to a constant matrix when the system becomes stable, which means that $\boldsymbol{err}(k)$ corrects $\boldsymbol{x}(k|k-1)$ in each sampling. When the speed or load torque changes suddenly, $\boldsymbol{K}(k)$ keeps still. In this situation, KO cannot adjust the parameters to the concrete speed and subsequently fails to obtain the optimally estimated speed. To overcome the shortcomings of KO, the measurement noise is calculated in real time by analyzing the position read by DSP, and a measurement noise SAKO is constructed in the following.

B. Real-Time Update of Measurement Noise

At low speeds, DSP may not read a new position in each sampling, and $T_1 > T_\mathrm{s}$. When DSP does not read a new position, the old position read by DSP in this sampling has a large error compared with the actual position, which means that the position read by DSP is incredible. Then, the measurement value $\theta(k)$ (the position in k_th time) should be ignored. There are two methods to ignore $\theta(k)$ in the state modification. One method assumes that the system model is very precise, i.e., $\boldsymbol{Q}(k) = 0$, and the other assumes that the measurement value is incredible, i.e., $R(k)$ is relative large. For a stable system, the system noise is constant; therefore, the measurement value should be ignored. This is to say that a large error exists between the position read by DSP and the actual position, and the measurement noise is large. Therefore, the measurement noise is set to be R_w, i.e., a large positive constant, which makes K small and approximately equal to zero. According to the first equation in (12), in this sampling, $\boldsymbol{x}(k|k)$ has a tendency toward $\boldsymbol{x}(k|k-1)$ and ignores $\boldsymbol{y}(k)$. In other words, the position read by DSP is not used to correct the estimated position, and SAKO is used as an estimator for position and speed.

When DSP reads a new position in this sampling, which means that the position read by DSP is credible, and then the measurement value at this moment should be considered in the state modification, the measurement noise is regarded as Gaussian white noise. Therefore, based on the actual situation, a small error whose maximum value is $e_\mathrm{max} = \min\{\hat{\omega}\,T_\mathrm{s}, \Delta\}$ exists between the position read by DSP and the actual position, where $\hat{\omega}$ is the mechanical angular velocity estimated by SAKO. As the measurement error is a stochastic variable that has no relationship with T_s, it can be regarded as a uniform probability distribution in the scope of $0 \sim e_\mathrm{max}$, and its distribution density is inversely proportional to the scope. The scope, expected error, and distribution density are respectively shown as follows:

$$\begin{cases} e \in [0,\ \min\{\hat{\omega}T_\mathrm{s},\ \Delta\}] \\ E\left[e(t)\right] = \frac{\min\{\hat{\omega}T_\mathrm{s},\ \Delta\}}{2} \\ f(e,t) = \frac{1}{\min\{\hat{\omega}T_\mathrm{s},\ \Delta\}} \end{cases} \tag{14}$$

where $e(t)$ is the measurement error; $E[e(t)]$ is the expected error; and $f(e,t)$ is the error distribution density.

According to (14), when DSP has read a new position at the current sampling, the measurement noise is calculated as follows:

$$R_t(t) = \min\left\{\frac{(\hat{\omega}T_\mathrm{s})^2}{12},\ \frac{\Delta^2}{12}\right\}.$$

The discrete form of the above equation is

$$R_t(k) = \min\left\{\frac{(\hat{\omega}(k|k-1)T_\mathrm{s})^2}{12},\ \frac{\Delta^2}{12}\right\}. \tag{15}$$

R_t calculated by (15) reflects the measurement noise between the position read by DSP and the actual position precisely when DSP reads a new position at different speeds. $\boldsymbol{K}$ calculated by R_t can use $\boldsymbol{err}(k)$ to correct $\boldsymbol{x}(k|k-1)$ and get a precise $\boldsymbol{x}(k|k)$. SAKO is used as an observer to observe state variables.

Above all, SAKO estimates state variables in each sampling but corrects them only when DSP reads a new position. Therefore, the estimate period of SAKO is T_s, and the error correct period is equal to T_1.

To sum up, the measurement noise of SAKO is shown as follows:

$$\boldsymbol{R}(k) = \begin{cases} R_t(k),\ \boldsymbol{y}(k) \neq \boldsymbol{y}(k-1) \\ R_w,\ \boldsymbol{y}(k) = \boldsymbol{y}(k-1). \end{cases} \tag{16}$$

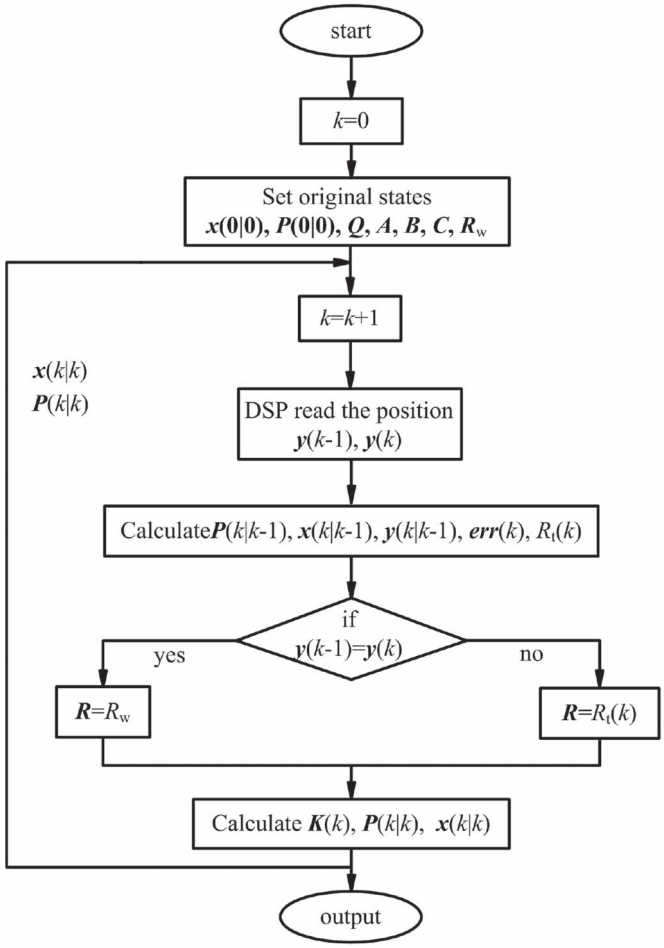

Fig. 2. Diagram of SAKO.

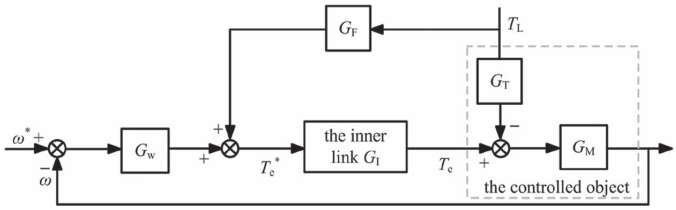

Fig. 3. Simplified block diagram of PMSM feedforward and feedback control.

$\boldsymbol{R}(k)$ is calculated timely in each sampling based on the estimate speed and the update of rotor position. Thus, the KO with the measurement noise self-adaption can observe the states precisely and timely when the motor speed is variant.

The calculation process of SAKO is shown in Fig. 2.

IV. Feedforward and Feedback Control of PMSM Based on SAKO

In the traditional feedback control system of speed and current PI controllers, the speed controller cannot follow speed timely and resist load disturbance at the same time when the motor load changes suddenly. In view of this problem, a feedforward and feedback control system is built by regarding the motor load as a system disturbance. Fig. 3 is the simplified block diagram of PMSM feedforward and feedback control.

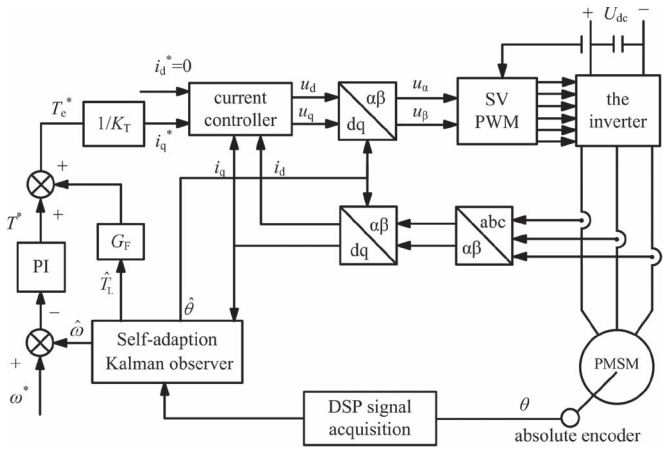

Fig. 4. PMSM feedforward–feedback control scheme.

In Fig. 3, G_{w} and G_{F} are the transfer functions of speed and feedforward controllers, respectively; G_{I}, which is approximately equal to one, is the transfer function of the inner loop; and G_{T} and G_{M} are the parameters of the motor model, i.e.,

$$\begin{cases} G_{\mathrm{M}} = \frac{1}{Js+f} \\ G_{\mathrm{T}} = 1. \end{cases}$$

In Fig. 3, the transfer function between speed and load torque is shown as follows:

$$\frac{\omega(s)}{T_{\mathrm{L}}(s)} = \frac{(G_{\mathrm{F}} + G_{\mathrm{T}}) \cdot G_{\mathrm{M}}}{1 + G_{\mathrm{w}} \cdot G_{\mathrm{M}}}.$$

In order to decrease the influence of load torque disturbance on speed, equation $G_{\mathrm{F}} = G_{\mathrm{T}} = 1$ should be established. Since the load feedforward controller and speed controller act on the PMSM system at the same time, the value of G_{F} needs to be chosen in the vicinity of 1 to achieve best speed control under the double effect of feedforward and speed controllers. The feedforward and feedback control system of PMSM shown in Fig. 4 is constituted by the feedforward compensation link and the speed feedback link. The feedforward compensation link consists of G_{F} and the load torque observed by the proposed observer.

In Fig. 4, a vector control strategy of $i_{\mathrm{d}} = 0$ with speed and current closed loops is used in PMSM; the rotor position, speed, and load torque are precisely observed by a limited precise absolute encoder and a SAKO; the observed signals are used as both speed feedback signals and compensation signal of load torque disturbance.

Within every sampling period, the SAKO can update measurement noise based on rotor position and its variations and adjust gain matrix timely; hence, the observed speed can reflect the actual speed of the motor accurately and timely. Based on this, when the observed speed is used as a feedback signal to control motor that runs in a dynamic condition, such as a sudden change of speed or load, etc., the speed PI controller can adjust the condition of the motor based on the observed speed timely, and then the control ability of the system is enhanced.

TABLE I
PARAMETERS OF THE MOTOR

parameter	value	unit
Pole-pair number p	24	
Stator resistance r	1.89	Ω
Stator inductor L_d=L_q	45.5	mH
Rotor flux linkage ψ_f	1.63	Wb
Rotational inertia J	3.0	kgm^2
friction torque coefficient f	0.05	(Nm)/(rad·s^{-1})
Rated torque T_N	1000	Nm
Rated speed n_N	50	r/min
Absolute encoder bit n	13	

V. Simulation and Experiment Analysis of the System

In the process of simulation and experiment, the parameters of the motor are listed in Table I. The control period of the system is $T = 100$ μs.

A. Simulation Analysis

In order to verify the performance of SAKO, the proposed system has been implemented in the MATLAB/Simulink programming environment. The system control period is $T = 100$ μs.

1) Property Test of SAKO: Known by [28], $\boldsymbol{x}(k|k)$ calculated by Kalman filter is the optimal estimation of the model state $\boldsymbol{x}(k|k)$ but not the optimal estimation of the real system state $\boldsymbol{x}^{\mathrm{r}}(k)$, and $\boldsymbol{P}(k|k)$ is only the estimation error covariance to $\boldsymbol{x}(k)$. Therefore, we need to consider the error covariance $\boldsymbol{P}^{\mathrm{r}}(k|k)$ between $\boldsymbol{x}^{\mathrm{r}}(k)$ and $\boldsymbol{x}(k|k)$ as a standard to judge the performance of Kalman filter. In certain conditions, the notion that the errors $\|\boldsymbol{x}^{\mathrm{r}}(k)-\boldsymbol{x}(k|k)\|^2$ have to be small to ensure that the Kalman filter is near optimal can be relaxed to requiring only that $\boldsymbol{P}^{\mathrm{r}}(k|k)$ and $\boldsymbol{P}^{\mathrm{r}}(k|k-1)$ (or their tracks) be small, and

$$\begin{cases} \boldsymbol{P}^{\mathrm{r}}(k|k-1) \\ \quad = E\left[\left(\boldsymbol{x}^{\mathrm{r}}(k)-\boldsymbol{x}(k|k-1)\right)\left(\boldsymbol{x}^{\mathrm{r}}(k)-\boldsymbol{x}(k|k-1)\right)^{\mathrm{T}}\right] \\ \boldsymbol{P}^{\mathrm{r}}(k|k) = E\left[\left(\boldsymbol{x}^{\mathrm{r}}(k)-\boldsymbol{x}(k|k)\right)\left(\boldsymbol{x}^{\mathrm{r}}(k)-\boldsymbol{x}(k|k)\right)^{\mathrm{T}}\right]. \end{cases}$$

In order to analyze the effect observed by KO more truly, the diagonal values of $\boldsymbol{P}^{\mathrm{r}}(k|k)$ are calculated, which represent the covariance value of the actual states and the observed states, i.e.,

$$\begin{cases} P_{11}^{\mathrm{r}} = E\left[(\theta^{\mathrm{r}}-\hat{\theta})(\theta^{\mathrm{r}}-\hat{\theta})^{\mathrm{T}}\right] \\ P_{22}^{\mathrm{r}} = E\left[(\omega^{\mathrm{r}}-\hat{\omega})(\omega^{\mathrm{r}}-\hat{\omega})^{\mathrm{T}}\right] \\ P_{33}^{\mathrm{r}} = E\left[(T_{\mathrm{L}}^{\mathrm{r}}-\hat{T}_{\mathrm{L}})(T_{\mathrm{L}}^{\mathrm{r}}-\hat{T}_{\mathrm{L}})^{\mathrm{T}}\right]. \end{cases}$$

Since the actual states of the system are not available in the experiment, the following Simulink is done in order to test and verify the performance of SAKO.

The motor system is controlled in a closed loop by the actual speed, the given speed is 30 r/min, and the motor starts up with no load and adds up a sudden load of 300 Nm at 0.25 s. Fig. 5(a) is the state error covariance of SAKO whose measurement noise is calculated by (15) and (16). Fig. 5(b) is the state error covariance of the traditional KO whose measurement noise adopts the adjustment value at the rated condition.

As shown in Fig. 5(a) and (b), the waveforms of P_{11}^{r} show that the position error covariances of the two methods are almost the same, which means that both methods can achieve to track the rotor position precisely. The waveforms of P_{22}^{r} and P_{33}^{r} show that, when the load changes suddenly, SAKO achieves to track speed and load in 0.02 and 0.015 s, respectively, whereas the traditional KO achieves to track speed and load in 0.045 and 0.04 s, respectively. The phenomenon is due to the fact that SAKO can update the system measurement noise and the gain matrix timely based on the speed . In summary, the time-variant measurement noise can reflect the noise in actual situation so that SAKO can track the variation of speed and load timely to make the response speed faster.

2) Speed Comparisons of Different Speed Measuring Methods: The given speed of the motor n^* is 30 r/min, the actual speed n is used for closed-loop control, the motor starts up with no load, and three traditional methods and two observers are all adopted to calculate the speed of PMSM.

The simulation result is shown in Fig. 6. n is the actual speed; n_1, n_2, n_3, n_4, and $\hat{n}$ are the speeds calculated by EM, PVM, POM, KO, and SAKO, respectively.

In Fig. 6(a), each method can calculate speed successfully although with speed errors at different levels. In Fig. 6(b), when the motor starts up, compared with the actual speed n, n_1 responds the fastest with the largest deviation. Compared with n_1, n_2, and n_3 have smaller deviations relatively but the slowest response speeds in the five methods. Moreover, n_4 and $\hat{n}$ can match n perfectly with the smallest speed deviations. In Fig. 6(c), when the motor runs steadily, the speeds calculated by the traditional methods have larger errors and need to be filtered, whereas KO and SAKO observe the speed with small errors. Among them, the speed observed by SAKO has the smallest error and gives the fastest response.

3) Simulation Results of the SAKO When the Load Changes Suddenly: The actual speed n is used for closed-loop control, the given speed $n^* = 30$ r/min, the motor starts up with no load, and the load increases to 300 Nm at 0.25 s. The speed $\hat{n}$ and load torque $\hat{T}_{\mathrm{L}}$ observed by the SAKO are shown in Fig. 7.

In Fig. 7, the speed and load torque are observed precisely and timely by the SAKO.

B. Experiment Analysis

The proposed SAKO is applied to a 10 kW low-speed and high-torque PMSM drive system to test its feasibility and validity. The experimental setup is shown in Fig. 8. The controller is chosen to be TMS320F28335 produced by Texas Instruments, its clock frequency being 150 MHz. Intelligent power modules Mitsubishi PM75DSA120 are utilized as power devices.

Although the proposed KO uses matrix multiplication to calculate speed, in order to decrease the amount of calculation, it is optimized in the experiment. The implementation process takes 9.5 μs, mainly to calculate 30 multiplications, 31 additions, and 1 division.

1) Speed Comparisons Between POM and the SAKO: In Fig. 6, among three traditional methods, the speed

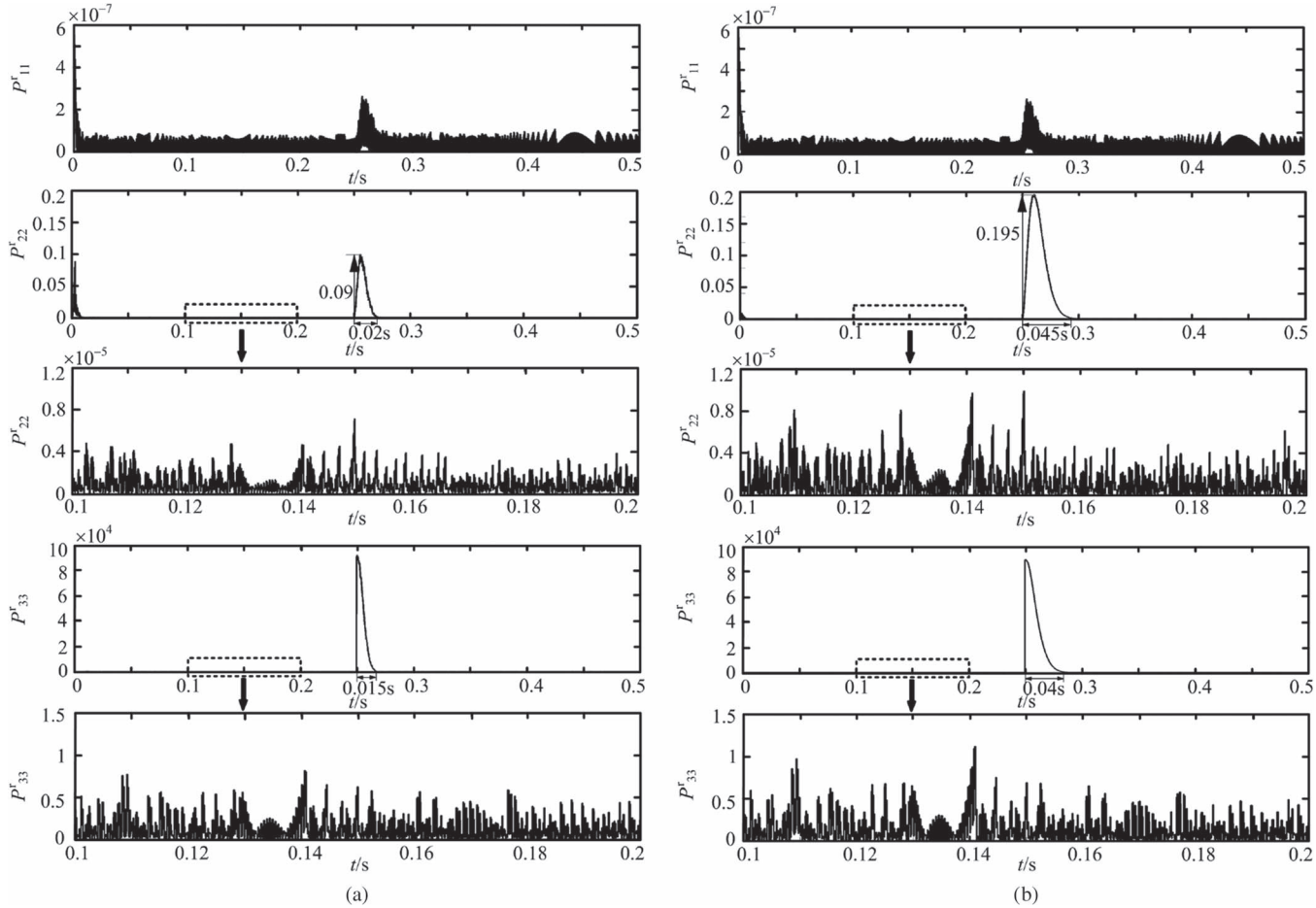

Fig. 5. State error covariances of SAKO and KO. (a) $\boldsymbol{P}^{\mathrm{r}}(k|k)$ of SAKO. (b) $\boldsymbol{P}^{\mathrm{r}}(k|k)$ of KO.

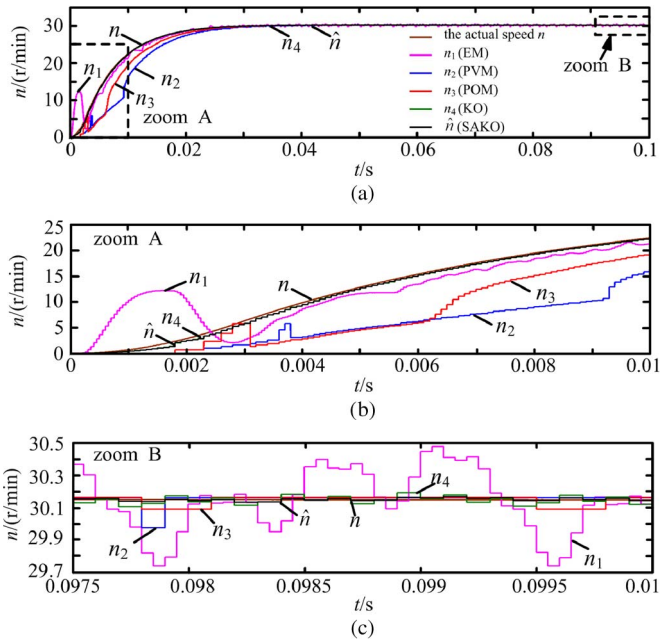

Fig. 6. Simulation of speed measurement. (a) Speed calculated by different methods. (b) Large chart when the motor starts up. (c) Large chart when the motor runs steadily.

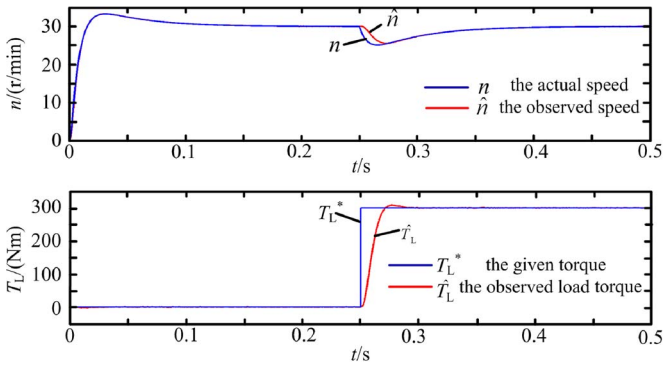

Fig. 7. Speed and load torque observed by SAKO.

calculated by POM has higher precision and faster response; thus, the speed calculated by POM n_3 is used to compare with $\hat{n}$ observed by SAKO. The motor controlled by n_3 starts up with no load. In order to analyze the response of SAKO, POM is at a high sampling rate, whose sampling period is $T_{\mathrm{s1}} = 100$ μs, whereas SAKO is at a low sampling rate, whose sampling period is $T_{\mathrm{s2}} = 1$ ms.

Fig. 9 shows the speed comparisons between two methods when the motor is in the conditions of starting up, running at variable speed, and forward and reversal. Fig. 9(a) is the comparison result when the motor starts up in the condition that $n^* = 30$ r/min; Fig. 9(b) is the comparison result when the motor runs in the condition that n^* changes from 10 to 30 r/min and then from 30 r/min back to 10 r/min suddenly; Fig. 9(c) is the comparison result that the motor runs in the condition that n^* changes from 30 to -30 r/min suddenly. $p\theta$, $p\hat{\theta}$, n_3, and $\hat{n}$

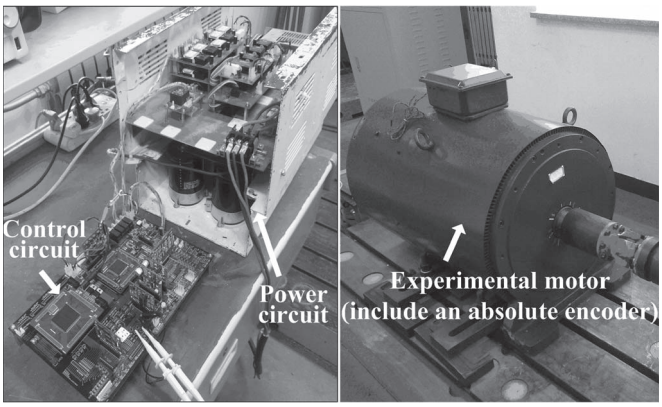

Fig. 8. Picture of the experimental setup.

are shown from top to bottom in each figure, where $p\theta$ and $p\hat{\theta}$ are the rotor electrical angles, and θ and $\hat{\theta}$ are the rotor positions read by DSP and observed by the SAKO, respectively.

In Fig. 9, at a low sampling rate, SAKO can observe both the rotor position and speed precisely and timely in above conditions, and the estimate accuracy and response speed are almost the same as those of POM at a high sampling rate. As shown in Fig. 9(c), at the moment of t_1, the direction of motor is just changing from forward to reversal; the actual speed is zero. The speed n_3 obtained by POM is 20 r/min at that moment and down to zero speed at t_2, which exists nearly 15 ms delay, whereas SAKO can observe the actual speed timely. Above all, the above experiment results verify the fast response and high accuracy of SAKO.

2) Closed-Loop Control of the Motor When the Given Speed is 30 r/min: The load torque increases from 0 to 300 Nm initially and then decreases to 0 Nm suddenly with $\omega^* = 30$ r/min and $T_{s1} = 100$ μs. Figs. 10 and 11 are respectively the response waveforms when the motor is closed-loop controlled by the speed calculated by POM and SAKO, respectively; Fig. 12 is the response waveform when the signals observed by SAKO are used to feedforward and feedback control of the system.

In Figs. 10–12, the motor can be controlled more precisely with a smaller speed ripple when the speed obtained by SAKO is used for feedback control compared with that by POM. At time t_1, the motor starts up, i_q increases fast, but the calculated speed n_3 by POM is obtained at t_2, which has nearly 7-ms delay, which causes larger fluctuation of i_q, whereas the speed $\hat{n}$ by SAKO is observed timely, and the fluctuation of i_q is smaller. The response time of that by SAKO is 0.1 s, whereas the response time of that by POM is 0.16 s. In addition, the SAKO can observe load torque precisely in nearly 0.15 s when the load changes suddenly, and the fluctuation of $\hat{n}$ caused by the variant load is decreased after using the feedforward controller.

3) Closed-Loop Control of the Motor When the Given Speed is 10 r/min: In order to compare the dynamic performance of POM and SAKO more impartially, three experiments have been done. Fig. 13(a) shows the response waveforms when the motor is closed-loop controlled by n_3 calculated by POM. Fig. 13(b) shows the response waveforms when the motor is closed-loop controlled by $\hat{n}$ observed by SAKO. Fig. 13(c) shows the response waveforms

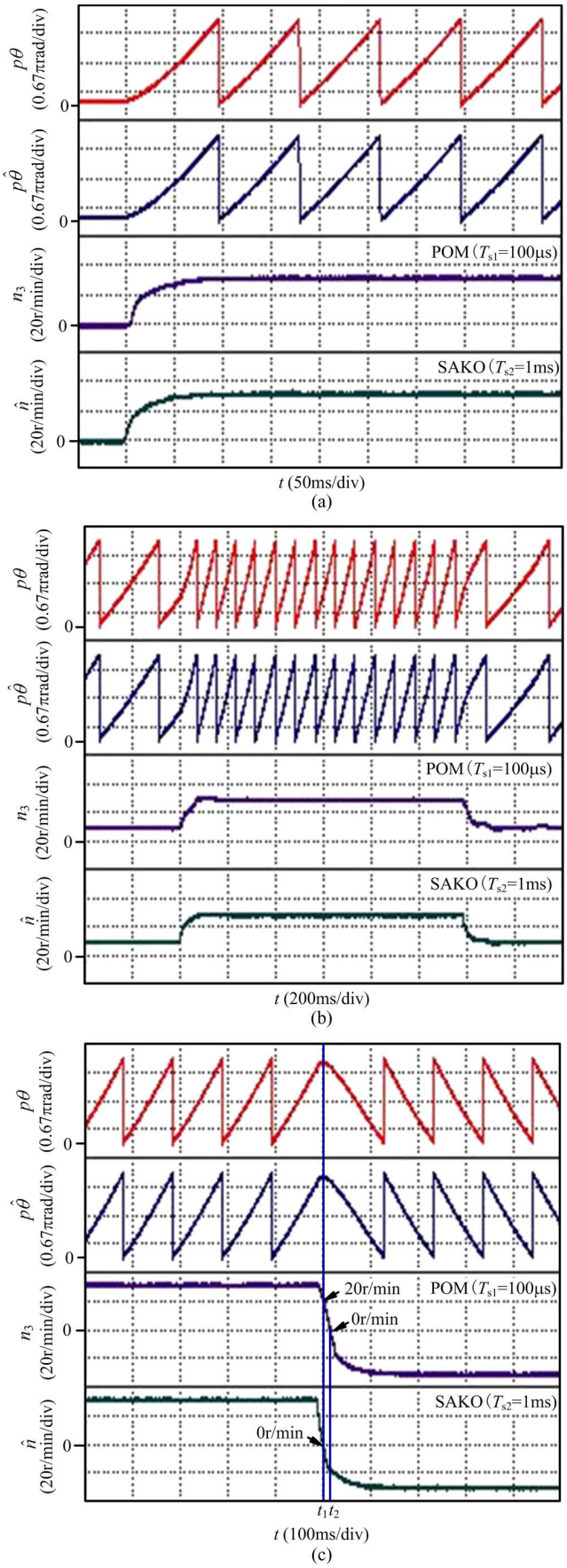

Fig. 9. Speed comparisons between POM and the SAKO: (a) start up; (b) variable speed; and (c) forward and reversal.

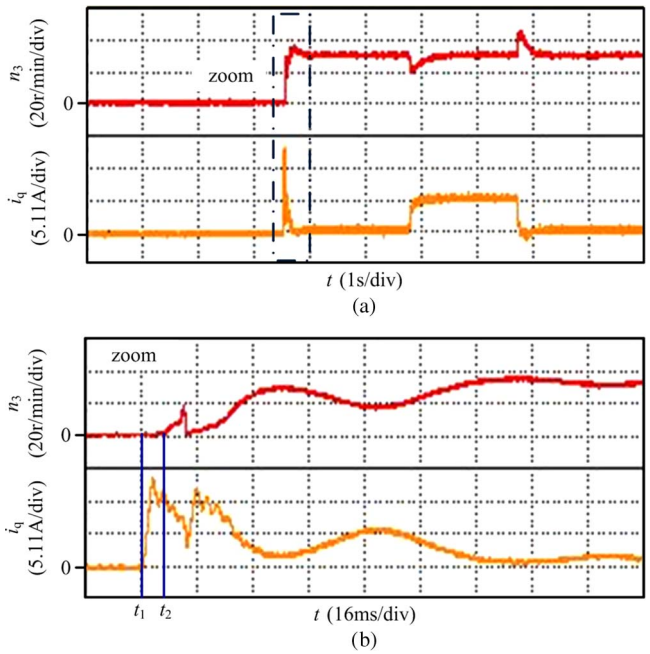

Fig. 10. Response waveforms when the speed calculated by POM is used for feedback control. (a) Waveforms of n_3 and i_q. (b) Enlarged waveforms when the motor starts up.

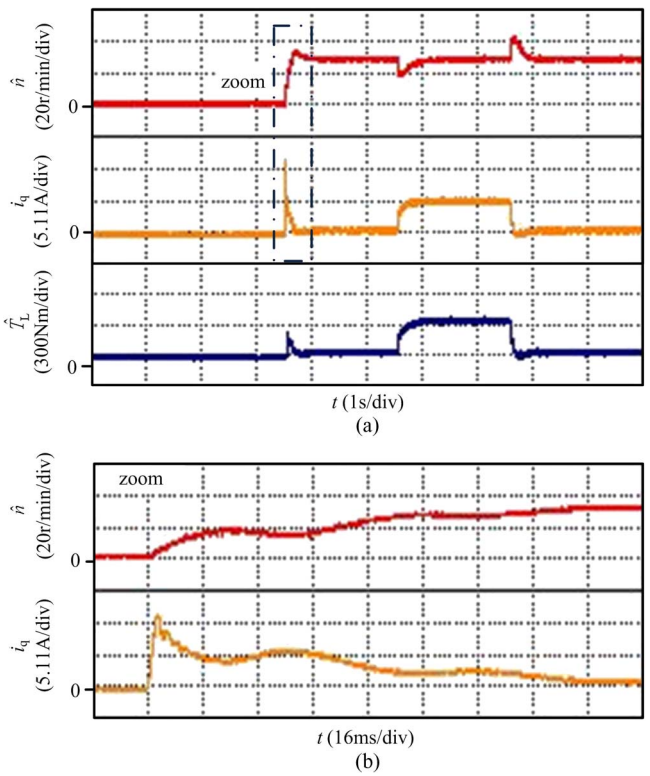

Fig. 11. Response waveforms when the speed obtained by SAKO is used for feedback control. (a) Waveforms of $\hat{n}$, i_q, and $\hat{T}_L$. (b) Enlarged waveforms when the motor starts up.

when the motor is feedforward and feedback controlled by $\hat{n}$ and $\hat{T}_L$ observed by SAKO. The given speed of the motor is 10 r/min, and the load torque increases from 0 to 300 Nm. To facilitate comparison, each experiment calculates the motor speed by POM and SAKO at the same time.

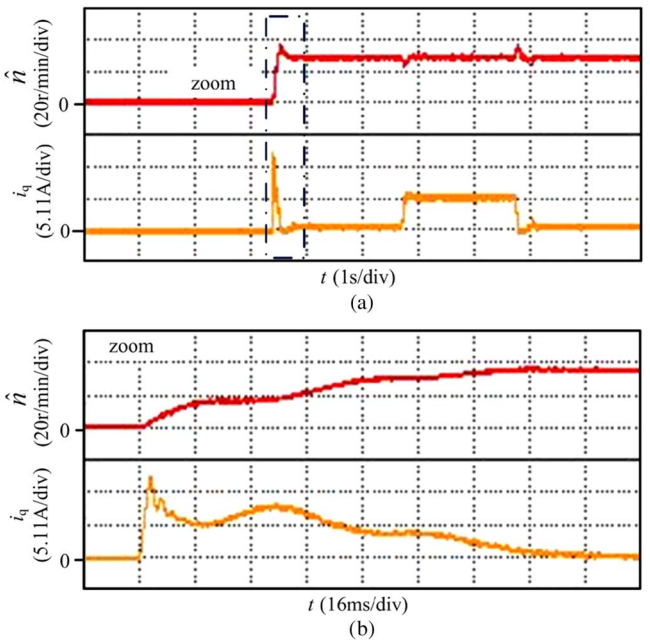

Fig. 12. Response waveforms when the motor is controlled by the feedforward and feedback controller. (a) Waveforms of $\hat{n}$ and i_q. (b) Enlarged waveforms when the motor starts up.

As shown in Fig. 13, the speed waveforms of POM and SAKO are both similar in each experiment. Compared with that of SAKO, the speed calculated by POM has nearly 20 ms time delay. It is further proved that SAKO can observe the actual speed more accurately without any time delay.

As the three experiments respectively use different control signals for the closed-loop control, their dynamic responses are different. If $\hat{n}$ is used to be compared in three experiments (the first waveform in each experiment), when load torque changes to 300 Nm suddenly and the control signal is n_3, i.e., the speed calculated by POM, which has nearly 20 ms time delay (compared with $\hat{n}$) and fails to reflect the actual speed of the motor timely, the speed PI controller then cannot adjust the condition of the motor timely leading to large speed drop and long recovery time (500 ms). Compared with POM, when $\hat{n}$, i.e., the speed observed by SAKO, is the control signal, it can reflect the actual speed accurately, and the recovery time (250 ms) is relatively shorter. As shown in Fig. 13(c), when $\hat{n}$ and $\hat{T}_L$ observed by SAKO are the control signals for feedforward and feedback control, the speed variation and the recovery time (100 ms) are further decreased. If n_3 is taken for comparison in the three experiments (the second waveform in each experiment), the conclusions are the same. In summary, when the motor runs at low speeds, since SAKO can observe $\hat{n}$ and $\hat{T}_L$ accurately and timely, the tracking performance and dynamic characteristic of the system are both improved to a certain extent.

VI. Conclusion

A SAKO has been proposed in this paper, which constructs a feedforward and feedback control system by combining with the motor model. Key conclusions are summarized as follows.

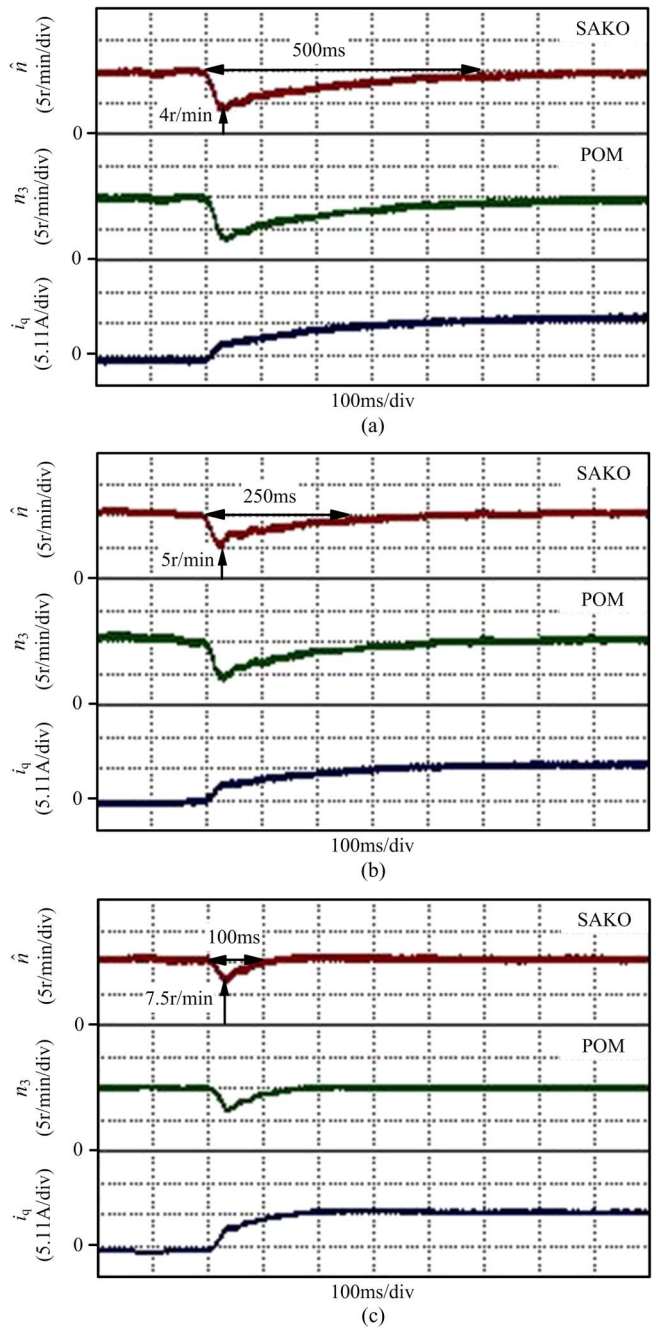

Fig. 13. Response waveforms at low speeds when the load torque changes suddenly. (a) n_3 is the control signal. (b) $\hat{n}$ is the control signal. (c) $\hat{n}$ and $\hat{T}_{\mathrm{L}}$ are the control signals.

1) Compared with the traditional speed measuring method, the proposed SAKO can observe both the rotor position and speed precisely and timely.
2) The motor can be controlled perfectly with a small speed ripple by the rotor position and speed observed by the SAKO; in addition, the fluctuation of i_{q} is decreased when the motor starts up.
3) The SAKO can identify the speed timely and precisely when the motor is in dynamic conditions; thus, the system controlled by $\hat{n}$ has a faster dynamic response performance.
4) The load torque observed by the SAKO can reflect the motor load timely. The speed tracking ability is improved by using the observed load torque as a feedforward compensation for the load disturbance.
5) For the motor equipped with an incremental encoder, it has similar position and speed measurement theories to that with an absolute encoder. Therefore, the design idea of the proposed SAKO is also applicable to a drive with an incremental encoder.

References

[1] J. M. Lopera *et al.*, "Practical speed and elongation measurement, using encoders, for a temper mill," *IEEE Trans. Ind. Appl.*, vol. 50, no. 1, pp. 113–119, Jan./Feb. 2014.

[2] R. C. Kavanagh, "Shaft encoder characterization via theoretical model of differentiator with both differential and integral nonlinearities," *IEEE Trans. Instrum. Meas.*, vol. 49, no. 4, pp. 795–801, Aug. 2000.

[3] N. Ekekwe, R. E. Cummings, and P. Kazanzides, "Incremental encoder based position and velocity measurements VLSI chip with serial peripheral interface," in *Proc. IEEE ISCS*, 2007, pp. 3558–3561.

[4] S. Wekhande and V. Agarwal, "High-resolution absolute position Vernier shaft encoder suitable for high-performance PMSM servo drive," *IEEE Trans. Instrum. Meas.*, vol. 55, no. 1, pp. 357–364, Feb. 2006.

[5] V. Liberali *et al.*, "A digital self-calibration circuit for absolute optical rotary encoder microsystems," *IEEE Trans. Instrum. Meas.*, vol. 52, no. 1, pp. 149–157, Feb. 2003.

[6] Y. Sugiyama *et al.*, "A 3.2 kHz, 14-bit optical absolute rotary encoder with a CMOS profile sensor," *Sensors J.*, vol. 8, no. 8, pp. 1430–1436, Aug. 2008.

[7] W. H. Zhu and T. Lamarche, "Velocity estimation by using position and acceleration sensors," *IEEE Trans. Ind. Electron.*, vol. 54, no. 5, pp. 2706–2715, Oct. 2007.

[8] S. M. Yang and S. J. Ke, "Performance evaluation of a velocity observer for accurate velocity estimation of servo motor drives," *IEEE Trans. Ind. Appl.*, vol. 36, no. 1, pp. 98–104, Jan./Feb. 2000.

[9] R. Petrella, M. Tursini, L. Peretti, and M. Zigliotto, "Speed measurement algorithms for low-resolution incremental encoder equipped drives a comparative analysis," in *Proc. Int. Aegean Conf. Elect. Mach. Power Electron.*, 2007, pp. 780–787.

[10] C. S. Wang, X. L. Li, L. Guo, and Y. W. Li, "A nonlinear-disturbance-observer-based DC-bus voltage control for a hybrid AC/DC microgrid," *IEEE Trans. Power Electron.*, vol. 29, no. 11, pp. 6162–6177, Nov. 2014.

[11] A. A. Prasov and H. K. Khalil, "A nonlinear high-gain observer for systems with measurement noise in a feedback control," *IEEE Trans. Autom. Control*, vol. 58, no. 3, pp. 569–580, Mar. 2013.

[12] C. P. Tan and C. Edwards, "Robust fault reconstruction in uncertain linear systems using multiple sliding mode observers in cascade," *IEEE Trans. Autom. Control*, vol. 55, no. 4, pp. 855–867, Apr. 2010.

[13] T. Bernardes, V. F. Montagner, H. A. Grundling, and H. Grundling, "Discrete-time sliding mode observer for sensorless vector control of permanent magnet synchronous machine," *IEEE Trans. Ind. Electron.*, vol. 61, no. 4, pp. 1679–1697, Apr. 2014.

[14] L. H. Zhao, J. Huang, H. Liu, B. Li, and W. Kong, "Second-order sliding-mode observer with online parameter identification for sensorless induction motor drives," *IEEE Trans. Ind. Electron.*, vol. 61, no. 10, pp. 5280–5289, Oct. 2014.

[15] Y. X. Su, C. H. Zhang, P. C. Mueller, and B. Y. Duan, "A simple improved velocity estimation for low-speed regions based on position measurements only," *IEEE Trans. Control Syst. Technol.*, vol. 14, no. 5, pp. 937–942, Sep. 2006.

[16] A. Accetta, M. Pucci, M. Cirrincione, and G. Vitale, "Neural sensorless control of linear induction motors by a full-order Luenberger observer considering the end-effects," *IEEE Trans. Ind. Appl.*, vol. 50, no. 3, pp. 1891–1904, May/Jun. 2014.

[17] M. A. Hamida, J. D. Leon, A. Glumineau, and R. Boisliveau, "An adaptive interconnected observer for sensorless control of PM synchronous motors with online parameter identification," *IEEE Trans. Ind. Electron.*, vol. 60, no. 2, pp. 739–748, Feb. 2013.

[18] L. Kovudhikulrungsri and T. Koseki, "Improvement of performance and stability of a drive system with a low-resolution position sensor by

multirate sampling observer," *IEEE Trans. Ind. Appl.*, vol. 12, no. 4, pp. 886–892, 2004.
[19] T. Tuovinen and M. Hinkkanen, "Signal-injection-assisted full order observer with parameter adaptation for synchronous reluctance motor drives," *IEEE Trans. Ind. Electron.*, vol. 50, no. 5, pp. 3392–3402, Sep./Oct. 2014.
[20] L. Harnefors and M. Hinkkanen, "Complete stability of reduced-order and full-order observers for sensorless IM drives," *IEEE Trans. Ind. Electron.*, vol. 55, no. 3, pp. 1319–1329, Mar. 2008.
[21] M. L. Corradini, G. Ippoliti, and S. Longhi, "A quasi-sliding mode approach for robust control and speed estimation of PM synchronous motors," *IEEE Trans. Ind. Electron.*, vol. 59, no. 2, pp. 1096–1104, Feb. 2012.
[22] Z. Yin, C. Zhao, Y. Zhong, and J. Liu, "Research on robust performance of speed sensorless vector control for the induction motor using an interfacing multiple-model extended Kalman filter," *IEEE Trans. Power Electron.*, vol. 29, no. 6, pp. 3011–3019, Jun. 2014.
[23] F. Alonge *et al.*, "Descriptor-type Kalman filter and TLS EXIN speed estimate for sensorless control of a linear induction motor," *IEEE Trans. Ind. Appl.*, vol. 50, no. 6, pp. 3754–3766, Nov. 2014.
[24] G. Rigators, P. Siano, and N. Zervos, "Sensorless control of distribution power generators with the derivative-free nonlinear Kalman filter," *IEEE Trans. Ind. Electron.*, vol. 61, no. 11, pp. 6369–6382, Nov. 2014.
[25] F. Alonge, T. Cangemi, F. D. Ippolito, A. Fagiolini, and A. Sferlazza, "Convergence analysis of extended Kalman filter for sensorless control of induction motor," *IEEE Trans. Ind. Electron.*, vol. 62, no. 4, pp. 2341–2352, Apr. 2015.
[26] R. C. Kavanagh and J. Murphy, "The effects of quantization noise and sensor nonideality on digital differentiator-based rate measurement," *IEEE Trans. Instrum. Meas.*, vol. 47, no. 6, pp. 1457–1463, Dec. 1998.
[27] A. B. Sripad and D. L. Snyder, "A necessary and sufficient condition for quantization errors to be uniform and white," *IEEE Trans. Acoust., Speech Signal Process.*, vol. 25, no. 5, pp. 442–448, Oct. 1977.
[28] B. Anderson and J. Moore, *Optimal Filtering*. Englewood Cliffs, NJ, USA: Prentice-Hall, 1979.

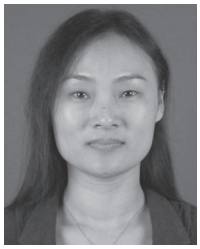

Tingna Shi (M'13) was born in Zhejiang, China, in 1969. She received the B.S. and M.S. degrees from Zhejiang University, Hangzhou, China, in 1991 and 1996, respectively, and the Ph.D. degree from Tianjin University, Tianjin, China, in 2009.

She is currently a Professor with the School of Electrical Engineering and Automation, Tianjin University. Her current research interests include electrical machines and their control systems, power electronics, and electric drives.

Zheng Wang was born in Hebei, China, in 1990. She received the B.S. degree in automation from Hebei University of Technology, Tianjin, China, in 2012. She is currently working toward the M.S. degree in automation in the School of Electrical Engineering and Automation, Tianjin University, Tianjin.

Her research interests include electrical machines and motor drives and power electronics.

Changliang Xia (M'08–SM'12) was born in Tianjin, China, in 1968. He received the B.S. degree from Tianjin University, Tianjin, in 1990 and the M.S. and Ph.D. degrees from Zhejiang University, Hangzhou, China, in 1993 and 1995, respectively, all in electrical engineering.

He is currently a Professor with the School of Electrical Engineering and Automation, Tianjin University, and also with the Tianjin Key Laboratory of Advanced Technology of Electrical Engineering and Energy, Tianjin Polytechnic University, Tianjin. In 2008, he became a "Yangtze Fund Scholar" Distinguished Professor and is currently supported by the National Science Fund for Distinguished Young Scholars. His research interests include electrical machines and their control systems, power electronics, and control of wind generators.